Comparison of the calculated and measured efficiencies of a normal-incidence grating in the 125-225 Å wavelength range

M. P. Kowalski, J. F. Seely, L. I. Goray, W. R. Hunter, and J. C. Rife

The efficiency of a diffraction grating was measured near normal incidence in the 125-225 Å wavelength range using synchrotron radiation. The grating pattern had 2400 grooves/mm and was recorded on a concave fused silica blank by a holographic technique. The grooves were shaped by ion beam etching to provide a facet with a blaze angle of 2.5^{o} as determined by atomic force microscopy. Because of the characteristics of the etching process, the groove profile was approximately triangular with the other facet inclined at an angle of 5.5^{o} to the surface. The measured efficiency was compared to the efficiency calculated by a computer program, small enough to run on a personal computer, that solved the periodic boundary value problem corresponding to electromagnetic radiation incident on a diffraction grating with finite conductivity. The calculation was based on the nominal groove profile that was determined by atomic force microscopy. The measured and calculated efficiencies were in good agreement. This work indicates that the diffraction efficiency of a normal-incidence grating can be calculated in the soft x-ray region using a personal computer.

L. I. Goray is with Integrate Inc., St. Petersburg, Russia. W. R. Hunter is with SFA Inc., 1401 McCormick Drive, Landover, Maryland 20785. The other authors are with the Naval Research Laboratory, Washington DC 20375-5352.

3 June 1997. Submitted to Applied Optics.

1. Introduction

The calculation of the energy that is diffracted into the orders of a grating requires the solution of the periodic boundary value problem corresponding to electromagnetic radiation incident on a diffraction grating. The calculation should account for the polarization of the radiation, the groove profile of the grating, and the finite conductivity of the grating surface.

Rigorous models for the solution of Maxwell's equations were developed by Maystre *et al.*[1] and Nevière *et al.*[2] and were based on the integral formalism and the differential formalism, respectively. These formalisms were discussed in detail in Ref. 3 and the references therein. Loewen *et al.*[4,5] used the integral and differential formalisms to calculate the normal-incidence efficiencies in the visible and ultraviolet regions of gratings with ideal blazed or sinusoidal groove profiles. Comparisons were made with the measured first order efficiencies of several gratings, and the agreement between the calculated and measured efficiencies was good.

Meekins *et al.*[6] used the differential method to calculate the grazing-incidence efficiencies in the 100-300 Å wavelength region of gratings with ideal laminar or blazed groove profiles. The gratings were produced by the ion-etched or ruled-replica techniques, and the gratings had gold coatings. The calculated efficiencies of the ion-etched gratings were in good agreement with the efficiencies that were measured using synchrotron radiation. However, the calculated efficiencies of the ruled-replica gratings differed significantly from the measurements, and this was attributed to the rather poor surface quality of the ruled-replica gratings that was not accounted for in the calculation.

Nevière[7,8] extended the differential formalism to include a multilayer coating on the grating. Calculations were presented for ideal blazed groove profiles and only for the polarization orientation with the electric vector parallel to the grooves.

Goray[9,10] recently developed a modified integral method that calculates grating efficiency in the ultraviolet and x-ray regions. This method reduces in a rigorous manner the problem of diffraction by a grating to the solution of coupled linear integral equations. The linear integral equations are reduced to a system of linear algebraic equations by the collocation method. In this method, the points of interpolation of the unknown functions are the same as the collocation points. Such an approach avoids additional difficulties connected with the re-normalization of the system. The best results are obtained by use of a segment-constant approximation of the integral expressions and equal length segments of integration. The number of members under the expression of the Greens function are equal approximately to the half-number of collation points. The fast convergence of the algorithm allows the calculation on a personal computer of the efficiencies of an arbitrary groove profile defined with a large number of points that account for the non-ideal shape and microroughness of the groove profile.

As discussed in Refs. 9 and 10, the results calculated using the modified integral method are in good agreement with other rigorous methods such as the differential method, the characteristic wave method, and the modal method. However, the most meaningful test of a computational method is the comparison with experimental data, and that is the purpose of the present work.

In this paper, we compare the calculated and measured normal-incidence efficiencies of an uncoated blazed grating in the 130-225 Å wavelength region. The

calculations were performed using the modified integral method of Refs. 9 and 10. The calculations were based on the nominal groove profile that was determined by atomic force microscopy. The calculated efficiencies were compared to the efficiencies that were measured using a monochromator and reflectometer at the National Synchrotron Light Source.

2. Atomic Force Microscopy

The grating was fabricated by Spectrogon UK Limited (formerly Tayside Optical Technology). The groove pattern was recorded, using a holographic technique, onto a fused silica (Spectrosil B) blank with a concave radius of curvature of 2.0 m. The pattern frequency was 2400 grooves/mm, and the pattern covered an area of size 45 mm by 35 mm. The sinusoidal groove profile was then ion-etched into the fused silica to produce a blazed groove profile with a desired blaze angle of 2.5^{o}. However, ion etching results in a groove profile closer to triangular than the ideal blazed (sawtooth) profile.

The groove profile was characterized using a Topometrix Explorer scanning probe microscope, a type of atomic force microscope (AFM). The probe was a supertip which was tapered to a size much less 0.1 μm. The AFM images were 500 pixels square with pixel sizes between 10 Å and 20 Å. Using standard Topometrix software, the images were leveled using a second-order polynomial fitting technique.

A typical AFM image recorded using 16 Å pixels is shown in Fig. 1, where the vertical scale has been exaggerated to reveal the texture of the groove surface. The microroughness, determined by integrating the power spectral density function over the 2

to 40 μm^{-1} spatial frequency range, was 3.2 Å rms. Most of the microroughness is concentrated at low spatial frequencies as is apparent in Fig. 1.

The central portion of the AFM image shown in Fig. 1 that covers one period of the grating pattern was selected for further study. An analysis program was written in the Interactive Display Language (IDL) for this purpose and will be discussed in detail in a future publication. The histogram of the pixel heights, for one period of the grating pattern, is shown in Fig. 2. The maxima at 10 Å and 85 Å in Fig. 2 are caused by rounding of the groove profile at the peaks and the troughs which is a result of the pattern fabrication process. An ideal groove profile, either sawtooth or triangular, would have a flat height histogram. The separation between the peaks in Fig. 2 represents the average groove height, approximately 75 Å.

The local blaze angle at each pixel was determined by using a least squares algorithm to fit a linear curve to the data points in a sliding window. The window was 25 pixels (400 Å) long in the direction perpendicular to the grooves and one pixel wide parallel to the grooves. The blaze angle is the arctangent of the fitted slope. The histogram of the blaze angles, for all rows of data in one period of the grating, is shown in Fig. 3. The peak at 2.5^o represents the classical blaze angle, and the peak at 5.5^o represents the steep facet of the ideal sawtooth profile as modified by the ion etching process.

For a density of 2400 grooves/mm and for facet angles of 2.5^o and 5.5^o, an ideal grating would have an groove height of 125 Å. However, the measured value of 75 Å (Fig. 2) indicates a significant degree of rounding at the peaks and troughs of the groove profile. In addition, the measured ratio of the heights of the 2.5^o and 5.5^o features in the

angle histogram (Fig. 3) is approximately 3, greater than the ratio of approximately 2 that is expected based on the average facet angles. The interpretation of the widths of the features in Fig. 3 is difficult because they are complicated functions of the surface roughness, the width of the sliding window, and the probe geometry. This will be addressed in a future publication.

The feature at -2^{o} in Fig. 3 results from the fits to the peaks and troughs of the groove profile, where the local slope is changing rapidly but has an average value near zero. Simulations show that the -2^{o} offset of this feature from zero is a consequence of the unequal average blaze angles of the two facets.

To provide a groove profile for the efficiency calculation, a representative AFM scan perpendicular to the grooves was chosen at random and scaled to the average groove height (75 Å). The resulting groove profile is shown in Fig. 4. This groove profile has 210 points.

3. Measured Efficiencies

The grating efficiency was measured using the Naval Research Laboratory beamline X24C at the National Synchrotron Light Source at the Brookhaven National Laboratory. The synchrotron radiation was dispersed by a monochromator that had a resolving power of 600.[11] Thin filters suppressed the radiation from the monochromator in the higher harmonics. The wavelength scale was established by the geometry of the monochromator and the absorption edges of the filters. Measurements were performed at 15 wavelengths

in the 125-146 Å range using a silicon filter and at 11 wavelengths in the 170-225 Å range using an aluminum filter.

The grating was mounted in a reflectometer that had precision sample and detector rotational motions.[12] For measurement, the grating was rotated so that the radiation was incident at an angle of 10^{o} to the normal to the grating surface. The grating was oriented so that the 5.5^{o} facets faced the incident radiation. Owing to the small angle of the opposite facets (2.5^{o}), the radiation also illuminated the facets that faced away from the incident radiation. In this orientation, the outside orders of the 2.5^{o} facet were close to the blaze condition. An area at the center of the grating approximately 1 mm in size was illuminated. The radiation was approximately 90% polarized with the electric field vector in the plane of incidence. In this orientation, the electric field vector was perpendicular to the grating grooves.

The detector was scanned in angle about the rotational axis of the reflectometer, and the diffracted energy was recorded by a Hammamatsu GaAsP photodiode at a sequence of fixed wavelengths. The grating efficiency was calculated as the ratio of the diffracted intensity to the incident beam intensity. A typical detector scan is shown by the data points in Fig. 5 for a wavelength of 146 Å, where the inside ($m>0$) and outside ($m<0$) diffraction orders are identified. The width of the orders was determined primarily by the detector slit which was 0.5^{o} wide in the dispersion direction.

The efficiencies were determined by fitting a background curve and five Gaussian profiles to the 0, ±1, and ±2 orders as shown by the solid curves in Fig. 5. The background and the five Gaussian profiles were fitted to the data points using a least squares technique. The background curve is a wavelength dependent artifact of the

reflectometer and was subtracted to obtain the true efficiencies. The heights of the Gaussian profiles (above the background curve) were determined for each of the detector scans that were performed at fixed wavelengths in the 125-225 Å range.

The efficiencies in the 0, ±1, and ±2 orders are shown by the data points in Fig. 6. Also shown is the total efficiency which is the sum of the efficiencies in the five orders. The measured efficiencies are plotted together in Fig. 7(a), where the crossings of the efficiencies as functions of wavelength are apparent. The -1 order has the highest efficiency at the longer wavelengths, and the -2 order has the highest efficiency at the shorter wavelengths. The crossing of the -1 and -2 orders occurs at a wavelength near 155 Å. The crossings of the +1 and ±2 orders occur in the 175-205 Å region.

4. Calculated Efficiencies

The solid curves in Fig. 6 and the curves in Fig. 7(b) are the calculated efficiencies. The efficiencies were calculated by the modified integral method described in Refs. 9 and 10. The calculations were performed using the nominal AFM groove profile shown in Fig. 4. Results were calculated for radiation that was incident at an angle of 10^{o} to the normal to the grating surface. The grating facets were oriented identically to that during the measurements, with the steeper facet (angle 5.5^{o}) facing the incident radiation. The electric field vector was perpendicular to the grooves. The calculation accounted for the finite conductivity of the grating surface, and the optical constants of fused silica (SiO_2) were derived from the compilation of Henke *et al.*[13]

The 0, ±1, ±2, ±3, ±4, and ±5 orders were included in the calculation. The efficiencies of the orders higher than $|3|$ were quite low. As shown by the solid curves in Fig. 6, the calculated efficiencies showed most of the features and tendencies of the measured values, although the calculations diverge to values greater than the measurements at longer wavelengths.

By comparing the measured and calculated efficiencies shown in Figs. 7(a) and 7(b), respectively, it is apparent that the wavelength positions of the crossings of the efficiency curves are well modeled. It is also apparent in Fig. 7 that the small calculated efficiency (<0.001%) of the +1 order at the shorter wavelengths is affected by detector noise, where the extremely small detected current (<1 picoamp) from the GaAsP photodiode is comparable to the background.

Additional calculations indicated that the wavelength positions of the crossings were very sensitive to the assumed height of the groove profile. For example, the crossing between the -1 and -2 orders occurred at wavelengths of 140, 155, and 165 Å for groove heights of 70, 75, and 80 Å, respectively. A similar shift to longer wavelengths of the crossings of the +1 and ±2 orders occurred with increasing groove height. This is consistent with the well-known increase in the blaze wavelengths with increasing groove height and blaze angle.

5. Conclusion

The primary result of this work is that the modified integral method described in Ref. 9 can be used to calculate the efficiency of a normal-incidence grating in the soft x-ray

region and with an arbitrary (non-ideal) groove profile. The duration of the entire calculation, consisting of 21 wavelengths and a groove profile with 210 points, was approximately two hours on a small personal computer (133 MHz Pentium with 16 MB RAM). In addition, this work shows that atomic force microscopy provides a realistic groove profile for such calculations.

Acknowledgments

Part of the work at the Naval Research Laboratory and at Integrate Inc. was supported by the Office of Naval Research 6.1 project "Application of Multilayer Coated Optics to Remote Sensing (AMCORS)." The NRL work was also partially supported by NASA projects W-18537 and W-18898. Part of the work was done at the National Synchrotron Light Source, which is sponsored by the Department of Energy under contract DEAC02-76CH00016. The authors thank David Turner of NRL Code 6930 for the use of the Topometrix AFM and Kai Stolt of Analytical Answers Inc. for additional AFM measurements.

References

1. D. Maystre, “Sur la diffraction d’une onde plane par un reseau metallique de conductivite finie,” Opt. Commun. **6**, 50-54 (1972).
2. M. Nevière, P. Vincent, and R. Petit, “Sur la theorie du reseau conducteur et ses applications a l’optique,” Nouv. Rev. Opt. **5**, 65-77 (1974).
3. R. Petit, ed., *Electromagnetic Theory of Gratings* (Springer-Verlag, New York, 1980).
4. E. G. Loewen, M. Nevière, and D. Maystre, “Grating efficiency theory as it applies to blazed and holographic gratings,” Appl. Opt. **16**, 2711-2721 (1977).
5. E. G. Loewen and M. Nevière, “Simple selection rules for VUV and XUV diffraction gratings,” Appl. Opt. **17**, 1087-1092 (1978).
6. J. F. Meekins, M. P. Kowalski, and R. G. Cruddace, “Efficiency measurements of reflection gratings in the 100-300 Å band,” Appl. Opt. **28**, 1369-1377 (1989).
7. M. Nevière, “Multilayer coated gratings for x-ray diffraction: differential theory,” J. Opt. Soc. Am. A **8**, 1468-1473 (1991).
8. M. Nevière, “Bragg-Fresnel multilayer gratings: electromagnetic theory,” J. Opt. Soc. Am. A **11**, 1835-1845 (1994).
9. L. I. Goray, “Numerical analysis for relief gratings working in the soft x-ray and XUV region by the integral equation method,” edited by R. B. Hoover and M. W. Tate, S.P.I.E vol. **2278**, 168-172 (1994).

10. L. I. Goray and B. C. Chernov, “Comparison of rigorous methods for x-ray and XUV grating diffraction analysis,” edited by R. B. Hoover and A. B. C. Walker, S.P.I.E vol. **2515**, 240-245 (1995).
11. J. C. Rife, H. R. Sadeghi, and W. R. Hunter, “Upgrades and recent performance of the grating/crystal monochromator,” Rev. Sci. Instrum. **60**, 2064-2067 (1989).
12. W. R. Hunter and J. C. Rife, “An ultrahigh vacuum reflectometer/goniometer for use with synchrotron radiation,” Nucl. Instrum. Methods **A246**, 465-468 (1986).
13. B. L. Henke, E. M. Gullikson, and J. C. Davis, “X-ray interactions: photoabsorption, scattering, transmission, and reflection at E=50-30,000 eV, Z=1-92,” At. Data Nucl. Data Tables **54**, 181-342 (1993).

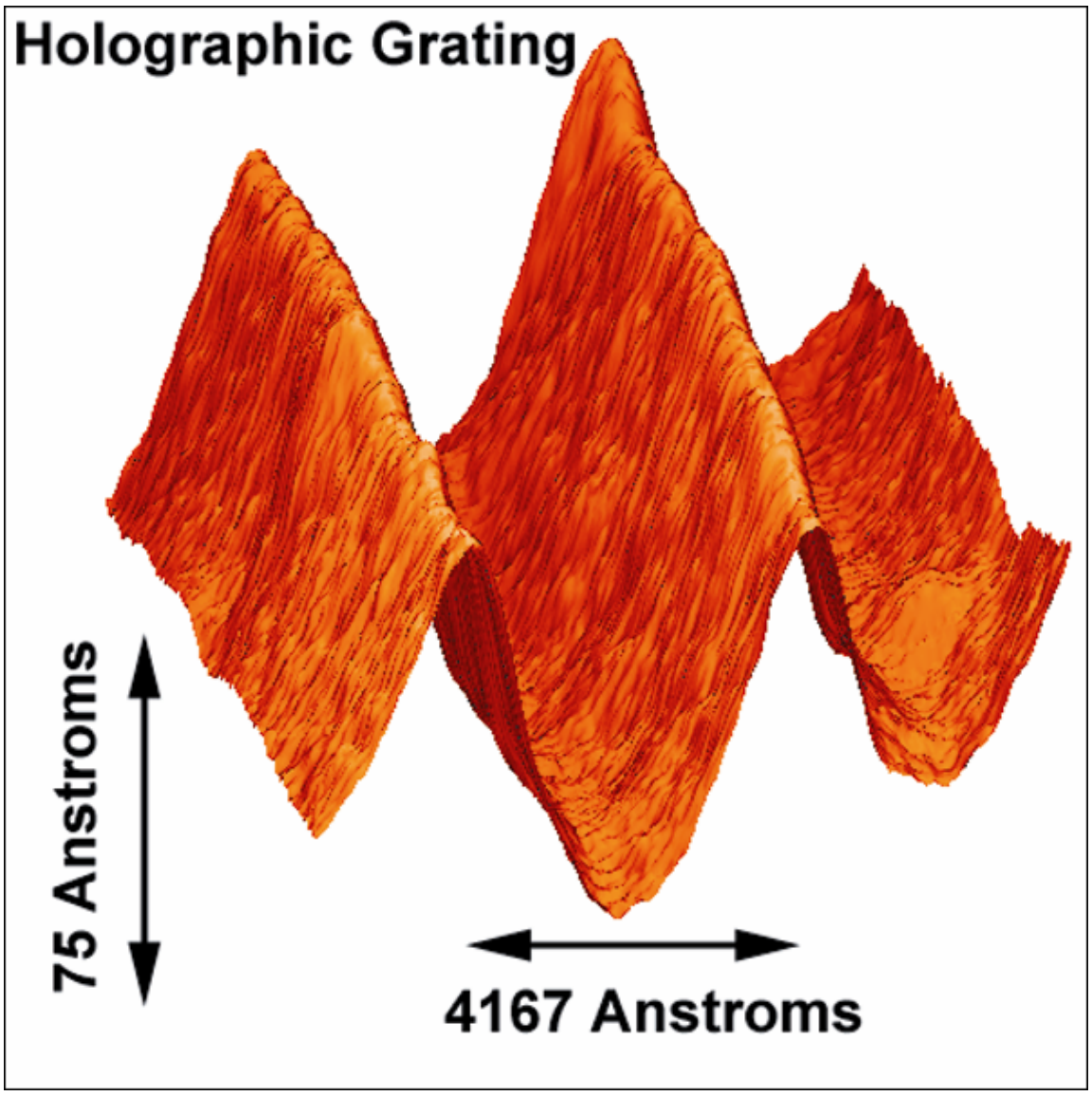

Fig. 1. The AFM image of the grating. The vertical scale has been exaggerated to reveal the texture of the grooves.

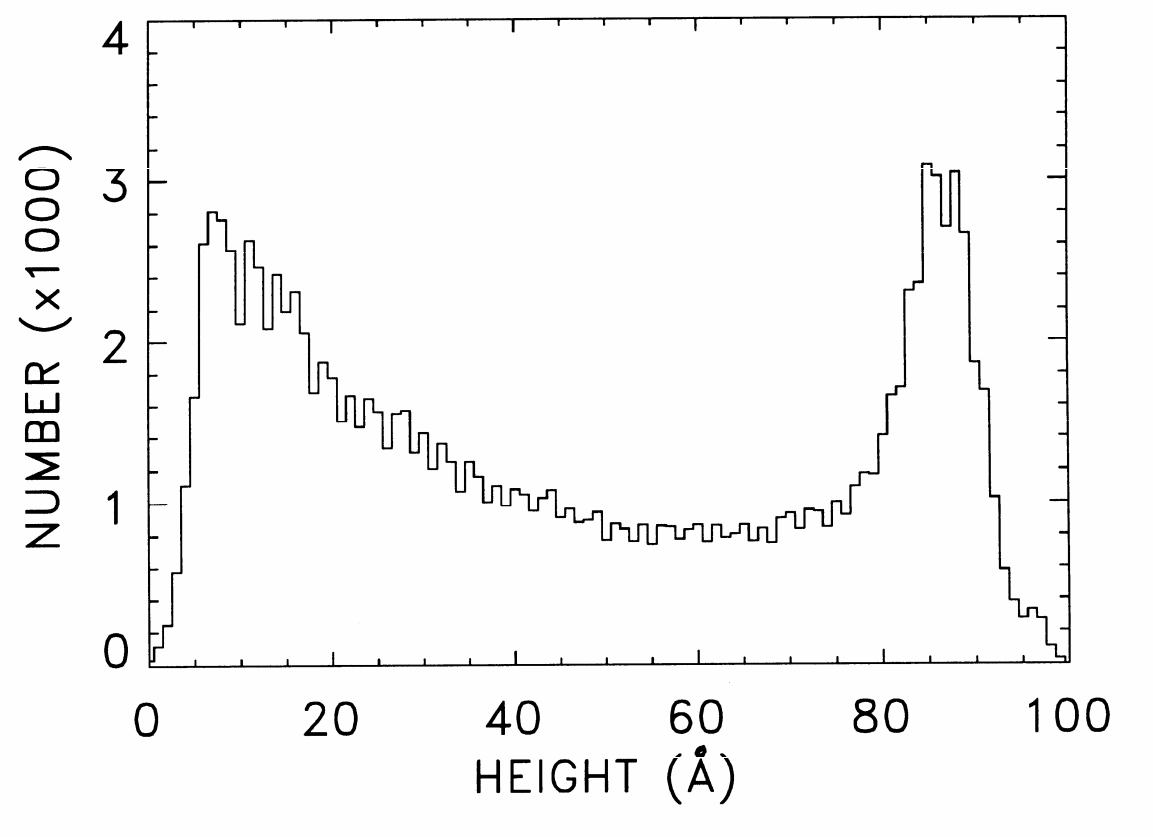

Fig. 2. The histogram of the pixel heights that were derived from one grating period of the AFM image.

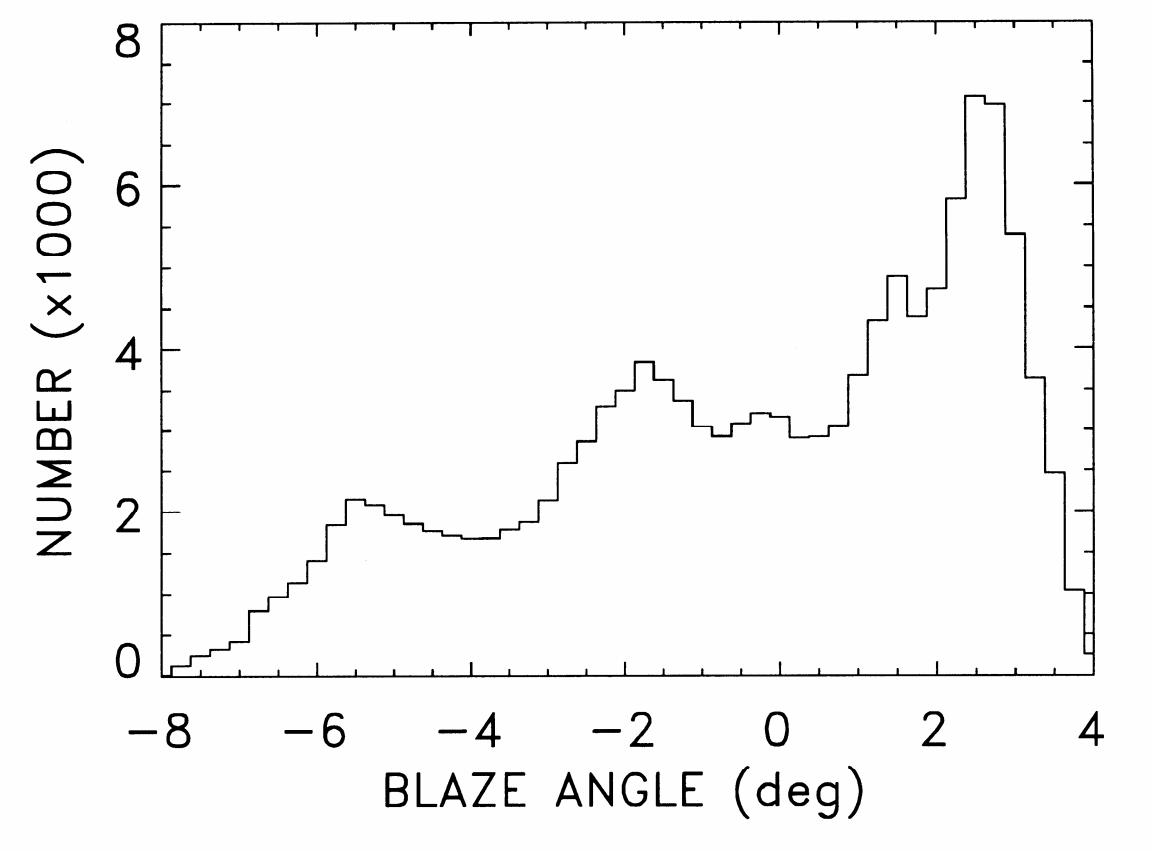

Fig. 3. The histogram of the blaze angles that were derived from one grating period of the AFM image.

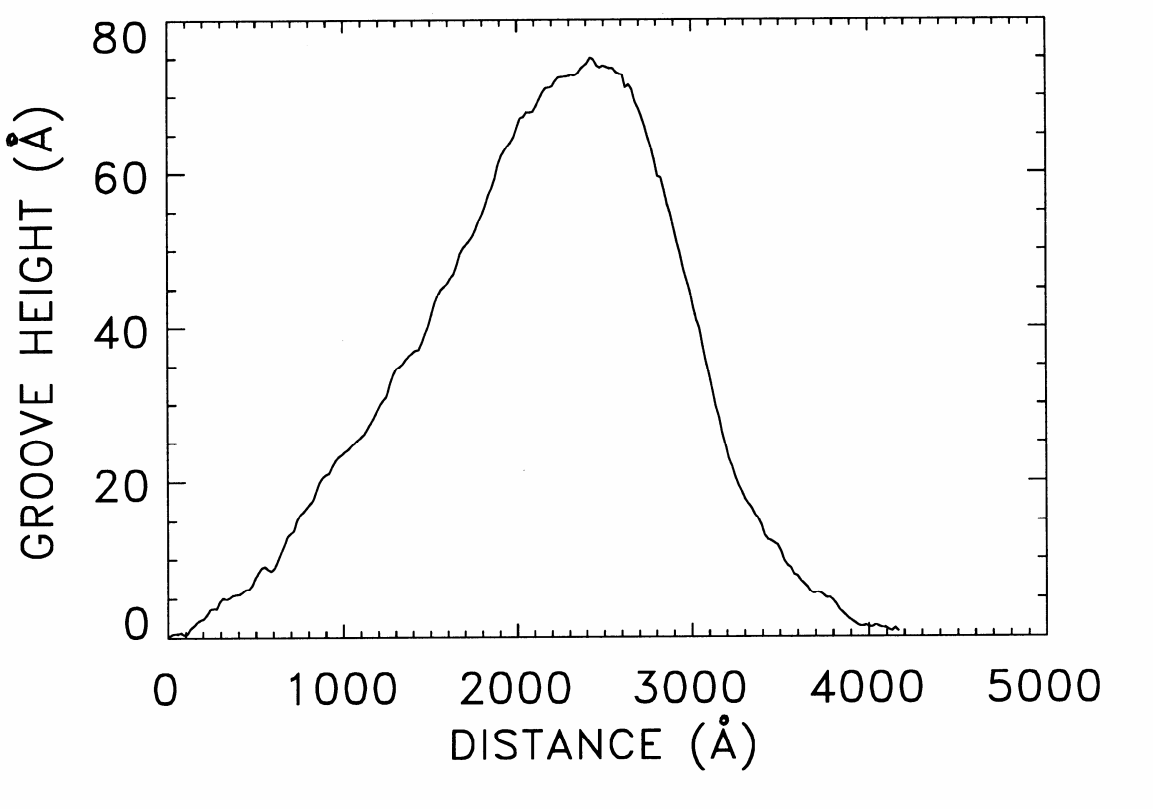

Fig. 4. A representative scaled groove profile that was derived from the AFM image and used in the calculation of the grating efficiency.

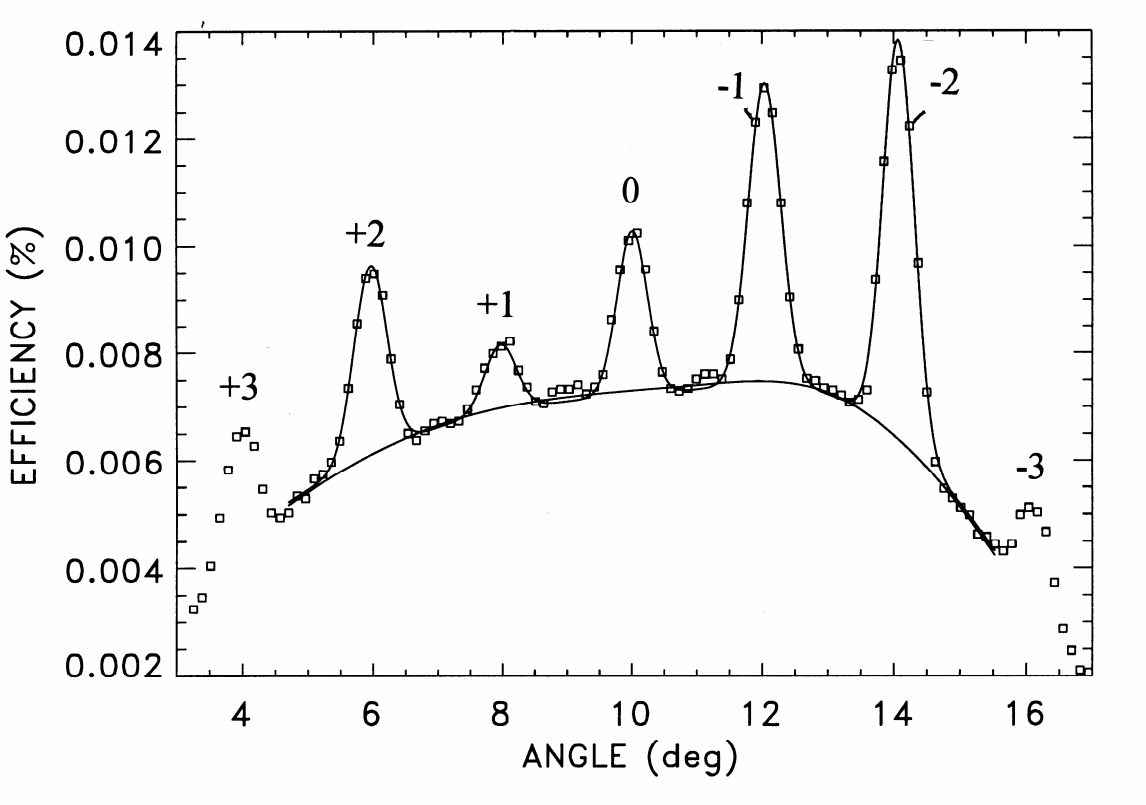

Fig. 5. The measured grating efficiency for a wavelength of 146 Å and an angle of incidence of 10^{o}. The inside (m>0) and outside (m<0) diffraction orders are indicated.

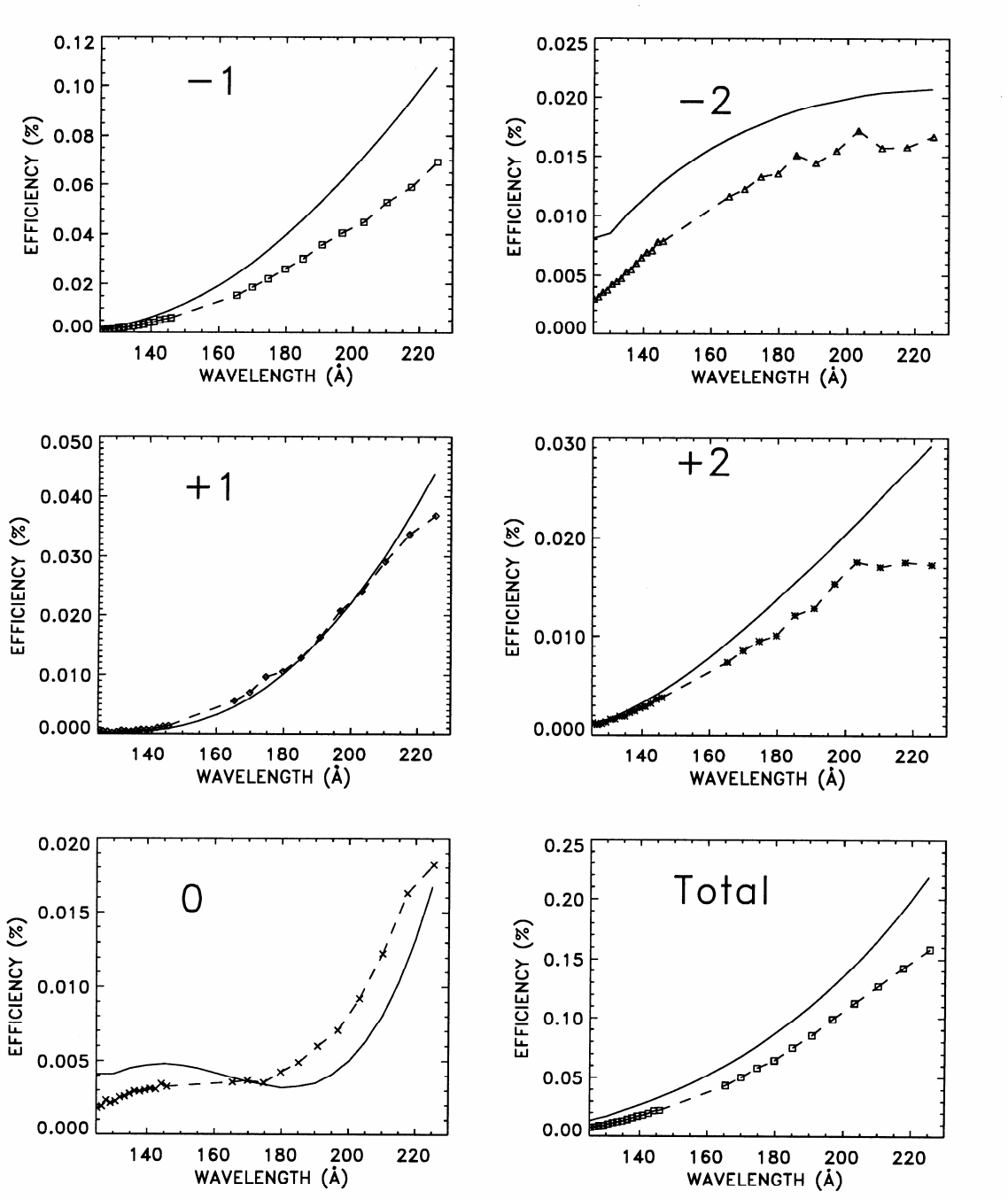

Fig. 6. Comparison of the measured (data points) and the calculated (solid curves) grating efficiencies for the indicated diffraction orders.

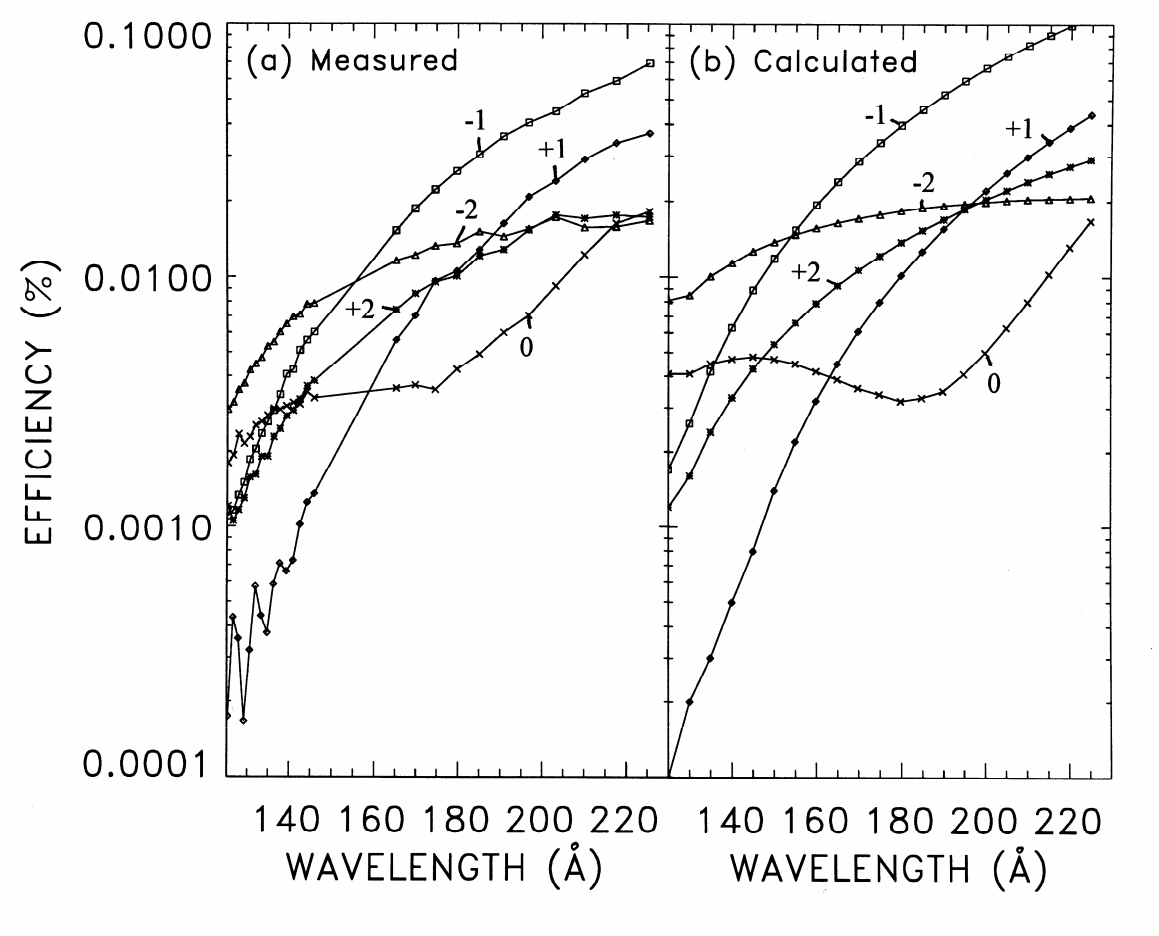

Fig. 7. Comparison of the (a) measured and (b) calculated grating efficiencies for the indicated diffraction orders.